J|A|C|S ARTICLES

Published on Web 09/15/2009

Unusual Electronic Structure of First Row Transition Metal Complexes Featuring Redox-Active Dipyrromethane Ligands

Evan R. King and Theodore A. Betley*

Department of Chemistry and Chemical Biology, Harvard University, 12 Oxford Street, 306E Mallinckrodt, Cambridge, Massachusetts 02138

Received May 16, 2009; E-mail: betley@chemistry.harvard.edu

Abstract: Transition metal complexes (Mn → Zn) of the dipyrromethane ligand, 1,9-dimesityl-5,5-dimethyldipyrromethane (dpm), have been prepared. Arylation of the dpm ligand α to the pyrrolic nitrogen donors limits the accessibility of the pyrrole π-electrons for transition metal coordination, instead forcing η^1,η^1 coordination to the divalent metal series as revealed by X-ray diffraction studies. Structural and magnetic characterization (SQUID, EPR) of the bis-pyridine adducts of (dpm)$Mn^{II}(py)_2$, (dpm)$Fe^{II}(py)_2$, and (dpm)-$Co^{II}(py)_2$ reveal each divalent ion to be high-spin and pseudotetrahedral in the solid state, whereas the (dpm)$Ni^{II}(py)_2$ is low-spin and adopts a square-planar geometry. Differential pulse voltammetry on the (dpm)$M^{II}(py)_2$ series reveals a common two-electron oxidation pathway that is entirely ligand-based, invariant to the divalent metal-bound, its geometry or spin state within the dpm framework. This latter observation indicates that fully populated ligand-based orbitals from the dpm construct lie above partially filled metal 3d orbitals without intramolecular redox chemistry or spin-state tautomerism occurring. DFT analysis on this family of complexes corroborates this electronic structure assignment, revealing that the highest lying molecular orbitals are completely ligand-based. Chemical oxidation of the deprotonated dpm framework results in the four-electron oxidation of the dipyrrolide framework, although this oxidation product was not observed either in the electrochemical or chemical oxidation of the (dpm)$M^{II}(py)_2$ complexes.

1. Introduction

Multielectron redox activity has long been associated with transition metal complexes with two or more accessible oxidation state changes (e.g., $M^n \rightarrow M^{n+1} \rightarrow M^{n+2}$). When the ligands that bind the transition metal ions can themselves operate as electron (or hole) reservoirs, the notion of accessible *molecular* redox states expands beyond that dictated by the metal's d-orbital electron configuration.[1] Redox activity has been attributed to a variety of ligand platforms (e.g., catechols,[2] dithiolates,[3] phenolates,[4] porphyrins,[5] bisimino-pyridines,[6] amidophenolates,[7] etc.) via their observed coordination chemistry and spectrochemical properties. The redox properties of the ligand platforms are being increasingly parlayed into driving new stoichiometric and catalytic reaction sequences. Redox-active ligands have most notably enriched the field of organometallic research with impacts ranging from bestowing multielectron reactivity to d^0 metals,[7] facilitating electronic interplay between metal and ligand during catalytic transformations,[6] and enabling dual-site reactivity during reaction sequences.[8]

Our own studies have focused on the coordination chemistry of dipyrromethane[9,10] and dipyrromethene[11] ligand frameworks as analogues to porphyrinogen and porphyrin scaffolds, respectively. The pyrrole aromaticity both attenuates the binding N π-basicity and makes them good candidates for ligand-centered redox activity by virtue of the high-lying π orbitals.[12] This

(1) Chaudhuri, P.; Verani, C. N.; Bill, E.; Bothe, E.; Weyhermüller, T.; Wieghardt, K. *J. Am. Chem. Soc.* **2001**, *123*, 2213–2223.
(2) Masui, H.; Lever, A. B. P.; Auburn, P. R. *Inorg. Chem.* **1991**, *30*, 2402–2410.
(3) (a) Schrauzer, G. N.; Mayweg, V. *J. Am. Chem. Soc.* **1962**, *84*, 3221. (b) Stiefel, E. I.; Waters, J. H.; Billig, E.; Gray, H. B. *J. Am. Chem. Soc.* **1965**, *87*, 3016–3017.
(4) (a) Hockertz, J.; Steenken, S.; Wieghardt, K.; Hildebrandt, P. *J. Am. Chem. Soc.* **1993**, *115*, 11222–11230. (b) Chaudhuri, P.; Hess, M.; Muller, J.; Hildenbrand, K.; Bill, E.; Weyhermuller, T.; Wieghardt, K. *J. Am. Chem. Soc.* **1999**, *121*, 9599–9610.
(5) Kadish, K. M., Smith, K. M., Guilard, R., Eds. *The Porphyrin Handbook*; Academic Press: San Diego, CA, 2003; Vols. 15−20.
(6) (a) Bouwkamp, M. W.; Bowman, A. C.; Lobkovsky, E.; Chirik, P. J. *J. Am. Chem. Soc.* **2006**, *128*, 13340–13341. (b) Bart, S. C.; Chlopek, K.; Bill, E.; Bouwkamp, M. W.; Lobkovsky, E.; Neese, F.; Wieghardt, K. *J. Am. Chem. Soc.* **2006**, *128*, 13901–13912. (c) Bart, S. C.; Lobkovsky, E.; Bill, E.; Wieghardt, K.; Chirik, P. J. *Inorg. Chem.* **2007**, *46*, 7055–7063.
(7) (a) Herebian, D.; Bothe, E.; Bill, E.; Weyhermuller, T.; Wieghardt, K. *J. Am. Chem. Soc.* **2001**, *123*, 10012–10023. (b) Blackmore, K. J.; Ziller, J. W.; Heyduk, A. F. *Inorg. Chem.* **2005**, *44*, 5559–5561. (c) Haneline, M. R.; Heyduk, A. F. *J. Am. Chem. Soc.* **2006**, *128*, 8410–8411. (d) Blackmore, K. J.; Lal, N.; Ziller, J. W.; Heyduk, A. F. *J. Am. Chem. Soc.* **2008**, *130*, 2728–2730.
(8) (a) Gunanathan, C.; Milstein, D. *Angew. Chem., Int. Ed.* **2008**, *47*, 8661–8664. (b) Gunanathan, C.; Shimon, L. J. W.; Milstein, D. *J. Am. Chem. Soc.* **2009**, *131*, 3146–3147. (c) Kohl, S. W.; Weiner, L.; Schwartsburd, L.; Konstantinovski, L.; Shimon, L. J. W.; Ben-David, Y.; Iron, M. A.; Milstein, D. *Science* **2009**, *324*, 74–77.
(9) (a) Jones, D. J.; Gibson, V. C. *Heterocycles* **2006**, *68*, 1121–1127. (b) Swartz, D. L.; Odom, A. L. *Organometallics* **2006**, *25*, 6125–6133.
(10) (a) Novak, A.; Blake, A. J.; Wilson, C.; Love, J. B. *Chem. Commun.* **2002**, 2796–2797. (b) Love, J. B.; Salyer, P. A.; Bailey, A. S.; Wilson, C.; Blake, A. J.; Davies, E. S.; Evans, D. J. *Chem. Commun.* **2003**, 1390–1391.
(11) King, E. R.; Betley, T. A. *Inorg. Chem.* **2009**, *48*, 2361–2363.
(12) (a) Floriani, C.; Floriani-Moro, R. In *The Porphyrin Handbook*; Kadish, K. M., Smith, K. M., Guilard, R., Eds.;Academic Press: San Diego, CA, 2000; Vol. 3, pp 405−420. (b) Bachmann, J.; Nocera, D. G. *J. Am. Chem. Soc.* **2004**, *126*, 2829–2837. (c) Bachmann, J.; Nocera, D. G. *J. Am. Chem. Soc.* **2005**, *127*, 4730–4743.

10.1021/ja903997a CCC: $40.75

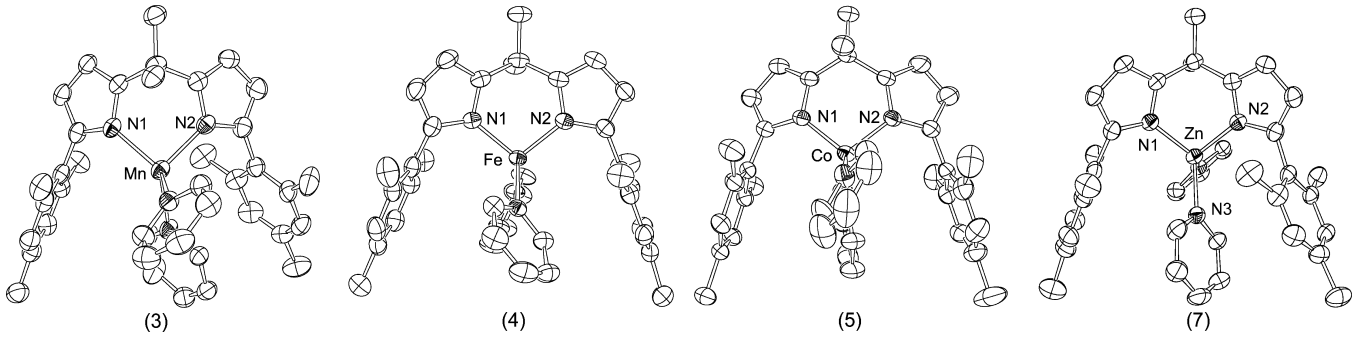

Figure 1. Solid-state molecular structures for complexes **3**, **4**, **5**, and **7** with the thermal ellipsoids set at the 50% probability level (hydrogen atoms and minor structural disorder in **3** and **4** are omitted for clarity).

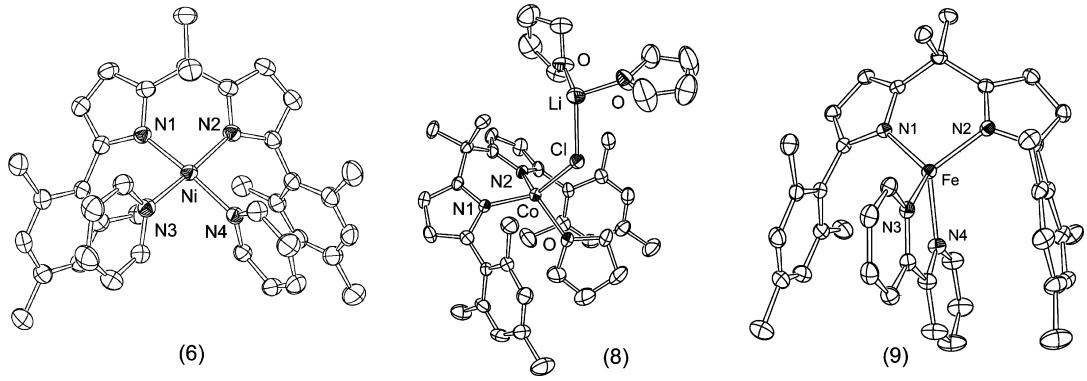

Figure 2. Solid-state molecular structures for complexes **6**, **8**, and **9** with the thermal ellipsoids set at the 50% probability level (hydrogen atoms, one solvent molecule for **6**, and two solvent molecules for **9** are omitted for clarity). The Li^+ in **8** is coordinated to an adjacent molecule's pyrrole ring.

contribution reports the synthesis and characterization of a series of divalent metal complexes of a dipyrromethane ligand. The complexes display surprisingly uniform electrochemical behavior despite differences in metal valence electron configuration as assessed by magnetic and spectroscopic methods, suggesting an interesting electronic structure which may involve intramolecular redox between the ligand and metal. Specifically, we consider three possible scenarios: (1) high-energy pyrrole-based electrons could reduce the bound metal ion filling the partially filled 3d orbitals with n e^-, leaving n holes on the ligand platform; (2) the ligand and metal-based orbitals are close enough in energy such that spin-state tautomerism is possible;[13] (3) no intramolecular redox occurs, leaving each metal in the divalent state with the ligand fully reduced. Our data lead us to favor the third scenario, wherein several fully populated ligand-based orbitals reside higher in energy than partially filled metal 3d orbitals, giving rise to a *non-Aufbau* electronic arrangement.

2. Results

2.1. Synthesis and Characterization of dpm and Its Metal Complexes. To assess the steric and electronic properties the 1,9-dimesityl-5,5-dimethyldipyrromethane dpmH$_2$ (**1**) ligand imparts, transition metal complexes were prepared in the following manner: Reaction of (dpm)Li$_2$(OEt$_2$) (**2**, prepared by deprotonation of **1** with two equivalents of PhLi) with a stoichiometric amount of a divalent metal precursor (i.e., $MCl_2(py)_2$; M = Mn, Co, Fe, Ni, Zn; py = pyridine) in thawing THF solutions afforded the metalated species of the type (dpm)M(py)$_2$ upon isolation via crystallization (M = pale-yellow Mn (**3**), bright orange Fe (**4**), maroon Co (**5**), crimson Ni (**6**), and yellow Zn (**7**)).

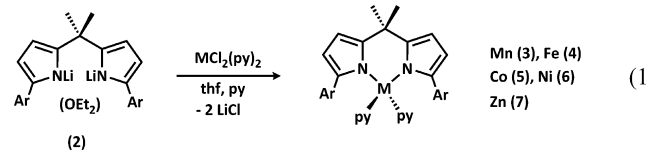

(1)

In the absence of strongly coordinating solvents, the formation of ate-complexes was observed (e.g., [(dpm)CoCl(THF)][Li(THF)$_2$] (**8**)). Substitution of the two pyridine ligands in **4** for 2,2′-bipyridine (bpy) results in the clean formation of (dpm)Fe^{II}(bpy) (**9**). The dpm ligand was found to uniformly coordinate in an η^1,η^1-coordination mode, accommodating both tetrahedral (observed for complexes **3**, **4**, **5**, **7**, and **8**) and square-planar coordination modes at the metal ion (observed for the diamagnetic Ni complex **6**) as confirmed by X-ray diffraction studies. The solid-state molecular structures for the tetrahedral Mn (**3**), Fe (**4** and **9**), Co (**5** and **8**), Ni (**6**), and Zn (**7**) complexes are shown in Figures 1 and 2.

2.2. Structural Characterization of Complexes 3−7. Complexes **3**−**5** and **7** are isostructural, featuring a pseudotetrahedral geometry at the metal center. The Ni complex **6** is distinct from this series, featuring a square-planar geometry at Ni. The metal pyrrolide nitrogen bond lengths decrease across the series of pseudotetrahedral complexes (d_{avg} (Å): Mn···N$_{dpm}$ = 2.053, Fe···N$_{dpm}$ = 1.982, Co···N$_{dpm}$ = 1.961, Zn···N$_{dpm}$ = 1.965; see Table SI-1, Supporting Information for a more comprehensive comparison of bond lengths). A similar trend is found when

(13) Storr, T.; Verma, P.; Pratt, R. C.; Wasinger, E. C.; Shimazaki, Y.; Stack, T. D. P. *J. Am. Chem. Soc.* **2008**, *130*, 15448–15459.

Table 1. Magnetic and Spectral Properties of Complexes **3**, **4**, **5**, and **9**

complex	S	μ_{eff} (BM)	λ/nm (ε/M$^{-1}\cdot$cm^{-1})	δ (mm/s)	ΔE_q (mm/s)
(dpm)Mn(py)$_2$ (**3**)	$^5/_2$	5.97,[a] 6.1(1)[b]	–	–	–
(dpm)Fe(py)$_2$ (**4**)	2	5.00,[a] 5.2(1)[b]	420 (1500), 1359 (70), 1675 (50) (sh)	0.80 0.86	3.46 2.63
(dpm)Fe(bpy) (**9**)	2	5.1(1)[b]	535 (410), 585 (620), 613 (870), 1125 (110), 1260 (105) (sh)	0.72	3.00
(dpm)Co(py)$_2$ (**5**)	$^3/_2$	4.20,[a] 4.5(1)[b]	395 (1100)	–	–
(dpm)Ni(py)$_2$ (**6**)	0	–	503 (190)	–	–

[a] Average moment over T range of 200−300 K from SQUID. [b] Room temperature (295 K) moment in solution by Evans's method.

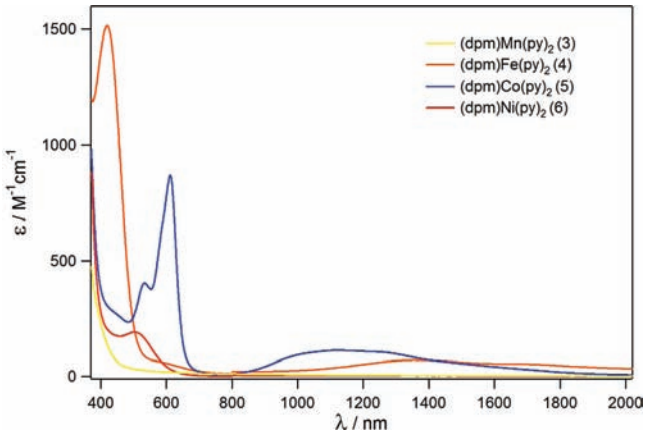

Figure 3. UV/vis/NIR molar absorptivity spectra of **3**, **4**, **5**, and **6**. Spectra were taken in dichloromethane, molar absorptivities are based on measurements at four concentrations.

comparing the metal pyridine nitrogen bond lengths (d_{avg} (Å): Mn···N$_{py}$ = 2.197, Fe···N$_{py}$ = 2.136, Co···N$_{py}$ = 2.045, Zn···N$_{py}$ = 2.087). In order to adopt the square-planar geometry in **6**, the Ni(py)$_2$ unit is brought out of the ligand plane (dihedral angle of 37° with respect to the pyrrolide subunits), further evidenced by the splaying of the two flanking mesityl aryl groups. The mesityl units of the dpm ligand carve a cleft about the Ni of 80.5°, defined as the angle formed by the two mesityl *ipso*-C atoms and the dpm bridgehead carbon atom ($\angle C_{ipso}-C_{Me2}-C_{ipso}$). This angle is consistent throughout the series, where angles of 77.6 (Mn), 86.6 (Fe), and 81.9° (Co) are observed.

2.3. Electronic and Magnetic Characterization of Complexes 3−7. The magnetic and spectral data for complexes **3**−**6** and **9** are provided in Table 1. The nearly colorless complex **3** has no transitions in the visible or near IR (NIR) regions (Figure 3) as expected for the ^{1}H NMR silent, high spin d^5 ($S = {}^5/_2$) Mn^{II} center (solution magnetic moment, μ_{eff} (295 K) = 6.1(1) μ_B). Based on the magnitude of their molar absorptivities, the visible absorptions for orange **4** (λ_{max}/nm (ε/M^{-1} cm^{-1}): 420 (1500)) and maroon **5** (λ_{max}/nm (ε/M^{-1} cm^{-1}): 613 (870)) are of the appropriate magnitude for spin-allowed d−d transitions for the high spin Fe^{II} ($S = 2$, μ_{eff} (295 K) = 5.2(1) μ_B) and Co^{II} ($S = {}^3/_2$, μ_{eff} (295 K) = 4.5(1) μ_B) centers in pseudotetrahedral ligand fields, respectively. Only very weak transitions are found for **4** (λ_{max}/nm (ε/M^{-1} cm^{-1}): 1359 (70), 1675 (50)) and **5** (λ_{max}/nm (ε/M^{-1} cm^{-1}): 1125 (110), 1260 (105)) in the near-IR region, which are too low in intensity to correspond to charge transfer bands (e.g., LMCT). Despite the paramagnetism of **4** and **5**, all nine proton resonances are discernible by ^{1}H NMR at 295 K ranging from δ 148 to −15 ppm. ^{1}H NMR analysis of **6** reveals several significantly broadened ($\Delta\delta$ = 1−2 ppm) resonances, yet no solution magnetic moment was measurable at room temperature, thus signifying the square-planar geometry observed in the low-temperature solid-state structure is preserved in solution. The observed broadening of the ^{1}H resonances can then be attributed to the limited motion of the mesityl aryl groups when accommodating the square-planar geometry. The relatively weak electronic transition observed for **6** (λ_{max} = 503 nm, ε = 190 M^{-1} cm^{-1}) is consistent with a Laporte forbidden d−d transition.

To confirm the high-spin character of complexes **3**−**5** at low temperatures, each complex was also characterized by SQUID magnetometry from 2−300 K and simulated with the julX package.[14] As can be seen from Figure 4, complexes **3**−**5** maintain their hextet (Mn **3**), quintet (Fe **4**), and quartet (Co **5**) ground states throughout this temperature range. The Curie Law observed for each complex in this temperature range (indicated by the linear plot χ_m^{-1} versus T, Figure 4b) indicates that the ascribed spin states are the only states thermally populated.[14] The powder EPR spectrum of **3** at 77 K reveals a complex multiline pattern consistent with multiple absorbances occurring for the high-spin Mn^{II} in a weak field ligand environment (Figure 5a). The powder EPR spectrum for the Co^{II} complex **5** exhibits an isotropic signal in the region of $g \approx 3.48$, consistent with high-spin Co^{II} ($S = {}^3/_2$), though the signal persists even to 298 K.[15] The EPR data for **5** was simulated using large zero-field splitting parameter D = 7.855 cm^{-1} and E/D = 0 as determined from fitting the SQUID data, with $g_\perp$ = 2.02, $g_{||}$ = 2.31.[16]

The Mössbauer spectrum of **4** shows multiple components modeled as two subspectra (Figure 6a). The two component subspectra have nearly identical isomer shifts (δ = 0.80, 0.86 mm$\cdot$s^{-1}) with different quadrupole splittings (component A: ΔE_Q = 3.46 mm$\cdot$s^{-1} (84%); component B: ΔE_Q = 2.63 mm$\cdot$s^{-1} (16%)), both consistent with Fe^{II} nuclei. The minor component grows in intensity the later the spectrum is acquired from the time of material preparation, even though ^{1}H NMR analysis does not reveal any change for the bulk material over a similar time frame. Analysis of **4** by ^{1}H NMR following Mössbauer measurements only reveals the (dpm)Fe(py)$_2$ complex without any observable decomposition (e.g., pyridine loss or dpm ligand dissociation). Neither subspectra are representative of the FeCl$_2$(pyridine)$_2$ starting material.[17] One possibility for the presence of two components could be structural isomers due to variation in pyridine binding to the Fe center.[17] The Mössbauer spectrum for **9** (Figure 6b), where the two pyridine ligands have been substituted for a single 2,2′-bipyridine ligand, reveals a single species featuring an isomer shift of 0.72 mm$\cdot$s^{-1} and a quadrapole splitting of 3.00 mm$\cdot$s^{-1}, consistent with the major component observed in the spectrum of **4**. The bipyridine ligand in **9** enforces a more acute $\angle$(N3−Fe−N4) bond angle (77.38°)

(14) Bill, E. julX: Simulation of Molecular Magnetic Data; available from http://www.mpi-muelheim.mpg.de/bac/logins/bill/julX_en.php, 2008.
(15) See Supporting Information for further physical characterization data.
(16) A similar modeling scheme was employed to model the EPR spectrum for a series of isoelectronic Cr(III) complexes. Pedersen, E.; Toftlund, H. *Inorg. Chem.* **1974**, *13*, 1603–1612.
(17) Long, G. J.; Whitney, D. L.; Kennedy, J. E. *Inorg. Chem.* **1971**, *10*, 1406–1410.

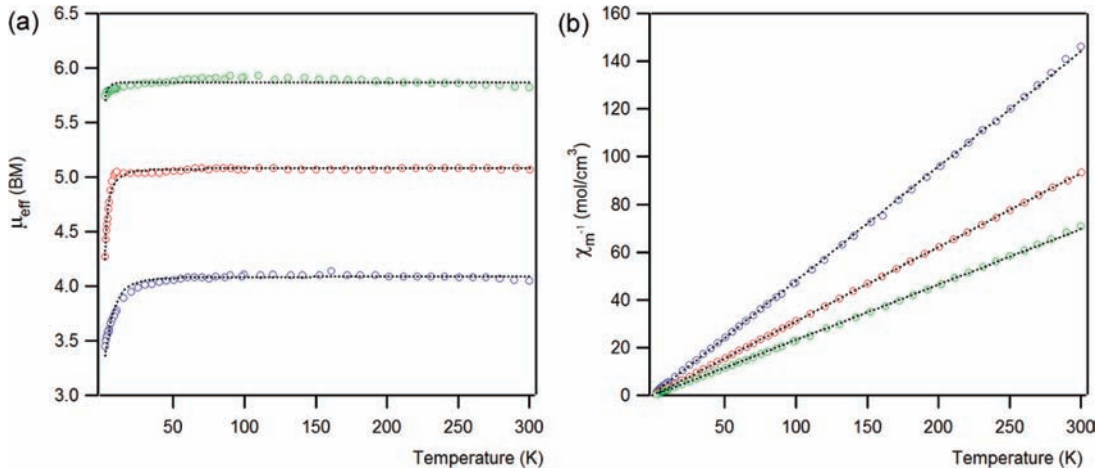

Figure 4. (a) SQUID magnetization data for complexes **3** (green ○), **4** (red ○), and **5** (blue ○) shown as a plot of μ_{eff} (BM) versus T (K) and (b) as a plot of χ_m^{-1} (mol/cm^3) versus T (K). Dotted lines are the simulations of each data set.[19]

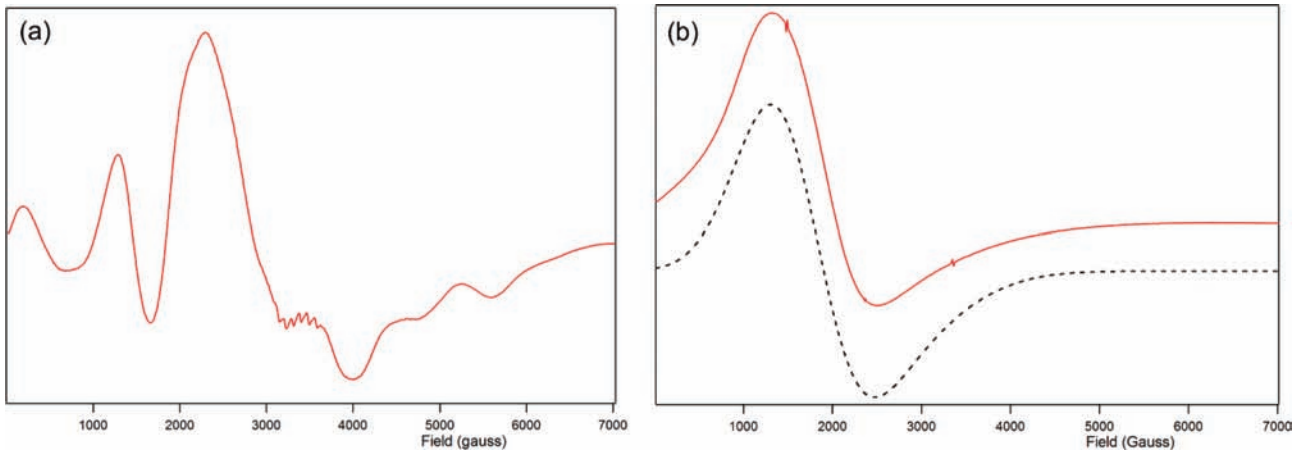

Figure 5. Powder EPR spectrum of (a) (dpm)$Mn(py)_2$ (**3**) and (b) (dpm)$Co(py)_2$ (**5**) (dotted line is data simulation: $g_\perp$ 2.02, $g_{||}$ 2.31; $A_\perp$ 0, $A_{||}$ 0.0112 cm^{-1}; D 7.855 cm^{-1}, E/D 0) (77 K, X-band, 9.397 GHz).

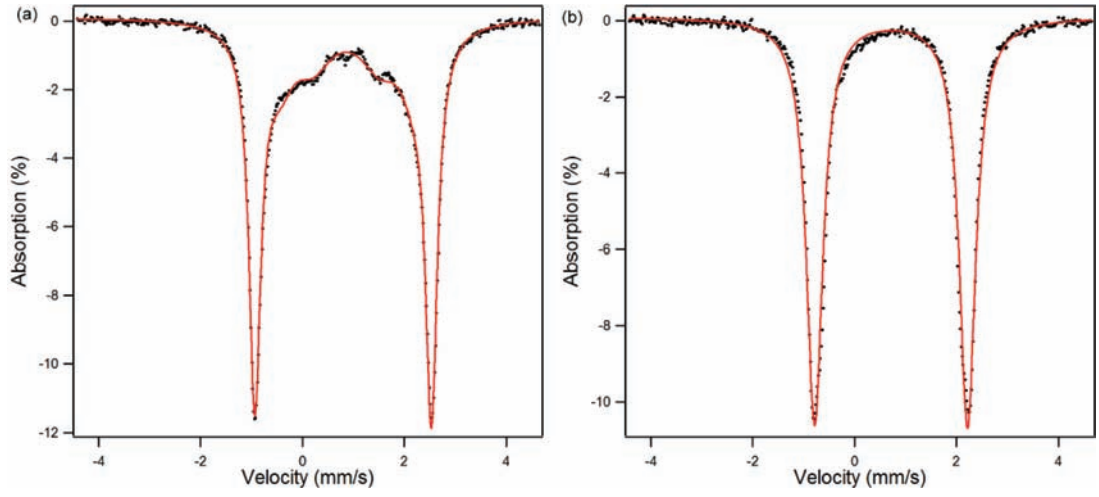

Figure 6. Zero-field Mössbauer spectrum of (a) (dpm)$Fe(py)_2$ (**4**) and (b) (dpm)Fe(bpy) (**9**) at 4.2 K.

as compared to the ∠(N3−Fe−N4) bond angle in **4** (97.32°). The large ΔE_Q for **9** is consistent with the greater deviation of **9** from an ideal tetrahedral geometry due to the bpy ligand. While the connectivity for **4** may not change, reorientation of the pyridine ligands in a more spherically symmetric fashion about Fe may produce the minor species detected in Figure 6a.

2.4. Electrochemical Behavior of Dipyrromethane Complexes. Cyclic voltammetry on the bis-pyridine complexes, **3**−**7**, showed no reversible oxidative or reductive events, and instead showed a rather complex series of irreversible oxidations. In order to probe their electrochemical behavior further, differential pulse voltammetry was used to assess the electrochemical potentials of these irreversible events. Using oxidative scans, all five

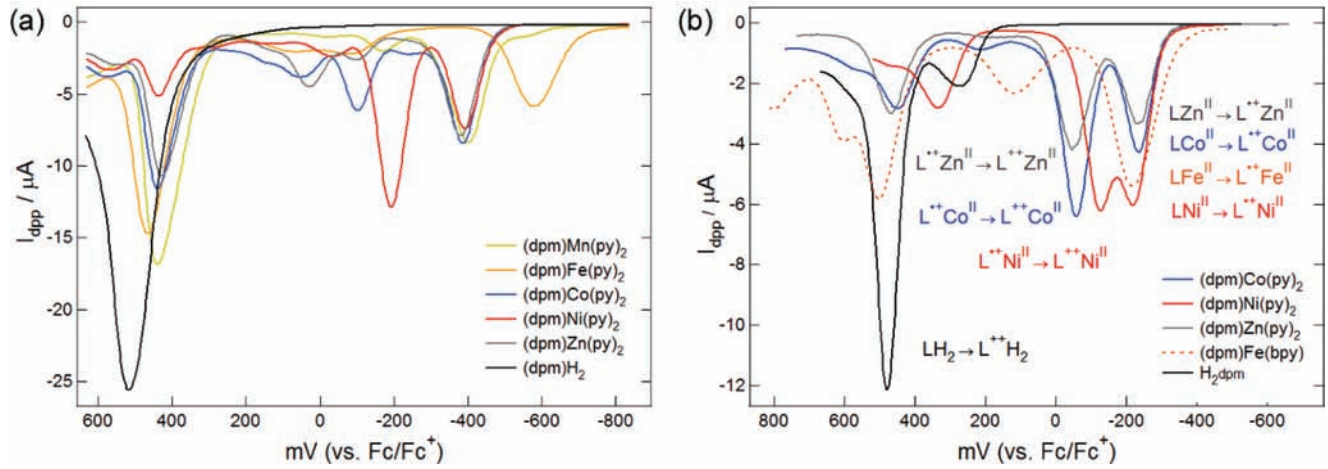

Figure 7. Differential pulse voltammograms of (a) solutions in THF of 10^{-4} M (dpm)M, where M = Mn(py)$_2$ (**3**), Fe(py)$_2$ (**4**), Co(py)$_2$ (**5**), Ni(py)$_2$ (**6**), Zn(py)$_2$ (**7**), H$_2$ (**1**); Bu$_4$NPF$_6$ (0.3 M); scan rate 20 mV/s on glassy C electrode), and (b) solutions in acetonitrile of 10^{-4} M (dpm)M, where M = Co(py)$_2$ (**5**), Ni(py)$_2$ (**6**), Zn(py)$_2$ (**7**), Fe(bpy) (**9**), H$_2$ (**1**); Bu$_4$NPF$_6$ (0.1 M); scan rate 20 mV/s on Pt electrode.

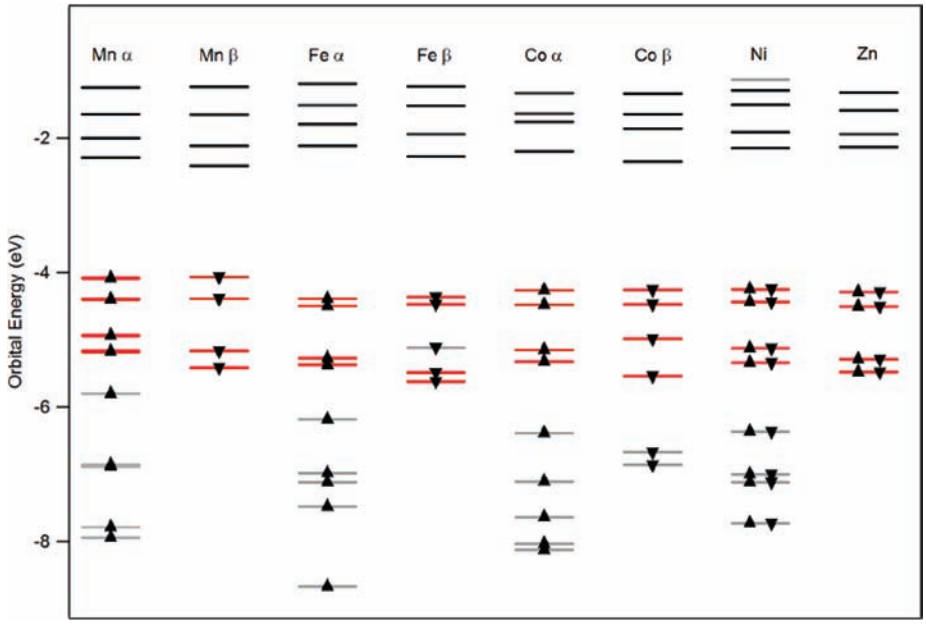

Figure 8. Calculated α (▲) and β (▼) orbital energies for Mn (**3**), Fe (**4**), and Co (**5**). Calculated molecular orbitals for Ni (**6**) and Zn (**7**). Metal-based orbitals are gray, dipyrromethane ligand-based orbitals are highlighted red, and pyridine-based orbitals are black.

species exhibited three major anodic peaks between −800 and +600 mV relative to Fc/Fc$^+$ in THF (0.3 M Bu$_4$NPF$_6$, Figure 7a). The potential of the initial peak corresponds well with the onset of current response in the cyclic voltammetry experiments, yet it was indeterminable if the oxidations represented one or two electron events. In acetonitrile solutions, the large oxidative waves for complexes **5**−**7** and **9** in THF separated into two well-defined one-electron events (Figure 7b). For 1 mM solutions of (dpm)M(py)$_2$ {M = Co (**5**), Ni (**6**), Zn (**7**)} and (dpm)Fe(bpy) (**9**) in acetonitrile (0.1 M Bu$_4$NPF$_6$, Pt working electrode) the initial peak was consistently observed at E_p = −240 mV. The Mn and Fe bis-pyridine complexes **3** and **4**, respectively, proved too labile in acetonitrile solutions to give reliable data. The Fe(bpy) analogue **9**, however, was stable enough in acetonitrile solutions to provide reproducible data, included in Figure 7b. The onset of oxidation for **9** is consistent with the Co (**5**), Ni (**6**), and Zn (**7**) species, although it does not exhibit a second oxidation event within a similar range. Subsequent peaks were observed at different potentials but followed similar patterns for all four metals. The Co and Zn voltammograms overlay with little deviation of the observed potentials, while the Ni voltammogram features the second one-electron oxidation at a slightly lower potential. We interpret the redox inactive Zn^{II} data to imply the observed sequential one-electron oxidations are predominantly ligand-centered. Interestingly, although the oxidations appear to be ligand-centered and vary little with divalent cation substitution, the onset of oxidation for metalated dpm does shift nearly 700 mV from the free dpmH$_2$ (E_p = 475 mV).

2.5. DFT Analysis. To further probe the electronic structure of the (dpm)M(py)$_2$ complexes, geometry-optimized calculations on the (dpm)M(py)$_2$ complexes **3**−**7** were performed (B3LYP/TZVP/SV(P)).[18] The orbital energies for complexes **3**−**7** are presented in Figure 8. Dipyrromethane orbitals are highlighted in red, metal 3d orbitals in gray, and pyridine orbitals are highlighted in black. In every instance the calculations indicate the highest lying occupied molecular orbitals (HOMO, HOMO−1) exclusively feature ligand π-character on the pyrrole

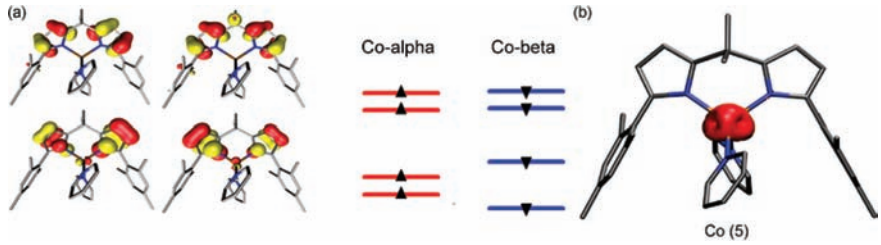

Figure 9. (a) HOMO to HOMO-4 from molecular orbital diagrams for **5** by DFT (B3LYP/TZVP/SV(P); Gaussian 03). (b) Calculated spin density for complex **5** (Co, $S = {}^3/_2$).

subunits, illustrated for complex **5** in Figure 9. The metal 3d-orbitals do not significantly contribute to the frontier orbitals until HOMO−4, often 1−2 eV lower in energy than the dipyrromethane-based HOMO. For the high-spin ion complexes **3**−**5**, the spin density plot ($\alpha-\beta$) reveals all of the spin localized on the metal ion (Figure 9b shows spin-plot for **5**). These results indicate that electron pairing within the higher-energy, delocalized dipyrromethane ligand π-orbitals is energetically favored over electron pairing within lower-energy, but localized metal ion 3d orbitals. This idea is consistent with encountering a significantly larger Coulombic repulsion for pairing electrons in 3d orbitals in the intramolecular redox state (dpm^{n+})M^{2-n} (scenario 1), than pairing electrons in energetically higher-lying, though diffuse dipyrromethane-based π-orbitals (scenario 3). The electronic structure suggested by the DFT results is consistent with the electrochemical behavior exhibited by complexes **3**−**9**. The pyrrolide π-electrons are the most accessible energetically; thus, we observe sequential pyrrole oxidation events with little perturbation by the chelated divalent ion.

2.6. Chemical Oxidation. Metal porphyrinogen complexes are known to undergo similar pyrrole-based oxidations (chemical and electrochemical), as shown by Floriani and Nocera.[12b,c] Sequential one-electron oxidations led to cyclopropane formation in the porphyrinogen's *meso* position via radical coupling of adjacent pyrrolic carbons in the 2 and 2′ position. Sequential one-electron oxidation of the two pyrrolide subunits should lead to a transient diradical, illustrated in eq 2.

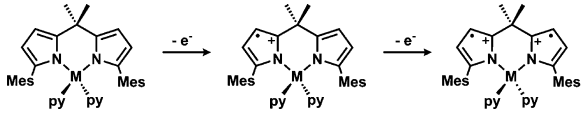

(2)

Whether the dipyrromethane ligands can undergo a radical coupling similar to the porphyrinogen platform to form a cyclopropane unit has yet to be confirmed. Chemical oxidation of the dilithio species **2** with two equivalents of AgCl in thawing THF solution produced one equivalent of free dpmH$_2$ **1** and an equimolar amount of a new diamagnetic species. ^{1}H NMR, HRMS, and X-ray crystallography confirm the new species obtained is the *four*-electron oxidized product diazacyclopentapentalene (**10**) (eq 3), which is inconsistent with two-electron oxidized, cyclopropane formation observed in porphyrinogen systems.

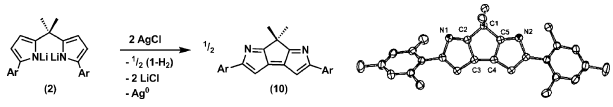

(3)

Presumably this process occurs from radical coupling of the ligand C3 and C7 positions followed by further two-electron oxidation and deprotonation. Coupling the pyrrole C3 and C7 positions, in this case, occurs preferentially to cyclopropane formation from the C4 and C6 positions, likely arising from carbocation stabilization at the pyrrolic C4 and C6 positions and radical localization at the pyrrolic C3 and C7 positions. Cyclic voltammetry on **10** in THF reveals only two reversible reduction events ($E_{1/2} = -1.14$ V, -2.28 V vs Fc/Fc$^+$), but no oxidation (Figure S1, Supporting Information). Chemical oxidation of complexes **3**−**6** with two equivalents of Fc$^+$PF$_6^-$ did not produce detectable quantities of **10**; only free ligand (**1**) and one equivalent of ferrocene were observed as the assignable products of oxidation. Likewise, attempts to directly synthesize a (dpm)M^{III} complex were unsuccessful. For example, metalation of M^{III} synthons (i.e., Mn^{III}(acac)$_3$, FeCl$_3$, Fe^{III}(acac)$_3$; acac = acetylacetonate) with **2** only yielded complex mixtures of (dpm)M^{II}(L)$_n$ species (L = pyridine, THF), free ligand, and unidentified metal salt mixtures, but no isolable (dpm)M^{III} materials.

3. Discussion

The most unusual feature of the complexes reported is the atypical electronic structure suggested by the electrochemical experiments. More precisely, the highest occupied molecular orbitals appear to be ligand based (see section 2.4), even for the complexes featuring high-spin electron configurations (**3**−**5**). The dipyrromethane *pyrrole π-electrons are thus higher in energy than the frontier orbitals of the 3d transition metal (Mn → Zn) investigated*, making intramolecular redox between the ligand and metal possible. Having fully populated ligand-based orbitals higher in energy than partially filled metal-based orbitals suggests that intramolecular redox is possible and might occur. We presented three possibilities for what types of intramolecular redox could be present, namely: (1) ligand-based electrons could reduce the bound metal ion, filling the partially filled 3d orbitals with n e$^-$, leaving n holes on the ligand platform; (2) the ligand and metal-based orbitals are closely matched in energy, and spin-state tautomerism is possible;[13] (3) no intramolecular redox occurs, leaving each metal in the divalent state with the ligand fully reduced.

Should electronic structure scenario 1 be operative, the dipyrromethane ligand structure should manifest stepwise oxidation with concomitant bond elongation within the pyrrole subunits,[12b,c] and the onset of oxidation in the electrochemical experiments should vary with metal ion substitution. Close inspection of all the bond lengths from the series of complexes **3**−**9** (Table SI-1, Supporting Information) does not reveal any perturbation of the dipyrromethane σ-bonds or π-bonds within the ligand architecture. The only significant variations discernible within the series are the bond lengths of M−N$_{dpm}$ and M−N$_{pyridine}$ (bonds 1−2 and 3−4, respectively, Table SI-1, Supporting Information) which vary due to the variable ionic size for the metals in different spin states. The invariant electrochemical behavior of metals bound by the dipyrromethane

ligand offer the most compelling evidence against scenario 1. Namely, the DPV experiments on the $(dpm)M^{II}(py)_2$ series reveal a common two-electron oxidation pathway that is entirely ligand-based, invariant to the divalent metal-bound (or its spin state) within the dpm framework. Moreover, the UV−vis/NIR results do not reveal a significant LMCT band, suggesting there are not even any excited states featuring charge transfer from the dpm to the M^{II} ions.

The SQUID magnetometry results cannot rule out any of the electronic structure postulates, as all three can be consistent with the total spin for each complex being preserved over the temperature range investigated. The EPR for both complex **3** and **5** are consistent for $S = {}^5/_2$ Mn and $S = {}^3/_2$ Co nuclei, respectively, with observed g values inconsistent for organic radicals, where $g \approx 2$. The EPR signals for both **3** and **5** persist over a broad temperature range (77−298 K). While this observation is unusual for typical Co^{II} ions in tetrahedral environments where fast spin−lattice relaxation times of the high-spin Co^{II} nucleus usually limit observation of transitions to below ∼30 K,[19] it also is inconsistent with spin-state tautomerism as a function of temperature.[13] The Mössbauer data for **4** and **9** suggest a single major nuclear environment for each of the Fe(II) ions and do not show any variance between 4 and 77 K. On the basis of the structural, electrochemical, and magnetic data, we rule out electronic structure scenarios 1 and 2 in favor of scenario 3 wherein no intramolecular redox is observed. This assignment is corroborated by the DFT analysis.

4. Conclusions

Transition metal complexes (Mn → Zn) of the dipyrromethane ligand 1,9-dimesityl-5,5-dimethyldipyrromethane (dpm) have been prepared. Arylation of the dpm ligand α to the pyrrolic nitrogen donors limits the accessibility of the pyrrole π-electrons for transition metal coordination, instead forcing η^1,η^1 coordination to the divalent metal ion. Electrochemical studies on the $(dpm)M^{II}(py)_2$ series reveal a common two-electron oxidation pathway that is entirely ligand-based, invariant to the divalent metal-bound (or its spin state) within the dpm framework. The energetically high-lying π-electrons from the dipyrromethane framework almost exclusively account for the observed redox behavior of the metal complexes studied. This latter observation indicates that fully populated ligand-based orbitals from the dpm construct lie above partially filled metal 3d orbitals without intramolecular redox chemistry or spin-state tautomerism occurring. This unusual electronic structure is corroborated by DFT studies, revealing fully occupied ligand-based π-orbitals at higher energies than half-filled metal 3d orbitals for Mn−Zn. While chemical oxidation of the $(dpm)M^{II}$ species did not yield a stable ligand-based diradical/dication, further experimental and computational studies are currently underway to elucidate the exact nature of the biradical generated as a result of both electrochemical and chemical oxidations.

Acknowledgment. We thank the American Chemical Society (PRF Grant Type G) and Harvard University for financial support, and Prof. R. H. Holm for the generous use of his Mössbauer spectrometer.

Supporting Information Available: Experimental procedures and details for complexes **1**−**10**. Cyclic voltammetry of **10** (Figure S1), χ_m vs T and $\chi_m{}^{-1}$ vs T for complexes **3**−**5** (Figure S2), X-band EPR of **3** and **5** at room temperature (Figure S3), DPV of complexes **3**−**7** and **9** in acetonitrile (Figure S4), dipyrromethane bond length comparisons (Table SI-1), X-ray diffraction experimental details for **3**−**10** (Table SI-2), complete reference 18 (SI endnote 9), and the geometry-optimized coordinates for complexes **3**−**7**. This material is available free of charge via the Internet at http://pubs.acs.org.

JA903997A

(18) (a) Frisch, M. J.; et al. *Gaussian 03*, Revision E.01; Gaussian, Inc.: Wallingford CT, 2004. (b) Weigend, F.; Ahlrichs, R. *Phys. Chem. Chem. Phys.* **2005**, *7*, 3297−3305.

(19) (a) Pilbrow, J. R. *Transition Ion Electron Paramagnetic Resonance*; Clarendon Press: Oxford, 1990. (b) Aasa, R.; Vänngård, T. *J. Magn. Reson.* **1975**, *19*, 308–315.